Journal of Hydrology 679 (2026) 136255

Contents lists available at ScienceDirect

Journal of Hydrology

journal homepage: www.elsevier.com/locate/jhydrol

Research papers

Climate-informed streamflow forecasting based on a Bayesian autoregressive exogenous stochastic volatility model and its use for hydrological drought forecasting

Pamela Sofia Fabian [a], Hemie Cho [b], Yoo-Geun Ham [c], Hyun-Han Kwon [a,*]

[a] Department of Civil Engineering, University of Seoul, Seoul, Republic of Korea
[b] Water Resources & Environmental Management Division, Korea Institute of Hydrological Survey, Goyang-si, Republic of Korea
[c] Department of Environmental Management, Graduate School of Environmental Studies, Seoul National University, Seoul, Republic of Korea

ARTICLE INFO

This manuscript was handled by Marco Borga, Editor-in-Chief

Keywords:
Bayesian autoregressive model
Climate state variable
Climate teleconnection
Drought index
Streamflow forecasting

ABSTRACT

In the context of South Korea's recurring drought challenges, this study explores season-ahead predictability of hydrological drought, focusing on Bayesian autoregressive modeling incorporating stochastic volatility. To better understand uncertainty, our approach integrates Bayesian inference and stochastic volatility, with comparisons of conventional autoregressive (AR), autoregressive with exogenous variables (ARX), and autoregressive exogenous with stochastic volatility (ARXSV) models. Our study explores the integration of climate-based information with statistical modeling, presenting a comprehensive framework for water resource management. We aim to predict June–July–August (JJA) streamflow and to assess the influence of large-scale climate predictors, such as the sea surface temperature and sea level pressure associated with the North Atlantic Oscillation. The methodology encompasses exploratory data analyses, the use of hydrological drought indices, and considerations related to dam operation. The research provides tailored season-ahead streamflow forecasts specifically for the critical monsoon season JJA, where hydrometeorological variability is paramount. By incorporating climate information within a Bayesian inference framework and stochastic volatility, we show that the proposed approach outperforms conventional autoregressive models, providing decision-makers with an efficient tool to address climate risk and support dam operation planning, ultimately contributing to improved water-resources management.

1. Introduction

Water resources management is vital for ensuring a stable and reliable water supply even in the face of natural climate variability and socio-economic pressures. Globally, dams and reservoirs play a critical role in addressing these challenges by capturing surplus water during wet seasons and releasing it during dry periods. In monsoon-dominated climate regions worldwide, recurrent hydroclimatic extremes such as droughts complicate effective reservoir operation; South Korea provides one illustrative example, where prolonged droughts (e.g., 1994–1995 and 2013–2016) posed major operational challenges (Jung et al., 2011; Kwon et al., 2016).

This emphasizes the importance of climate variability during the summer monsoon season, which runs from June to August (JJA) and accounts for 60–80% of South Korea's annual precipitation (Hong et al., 2016; Myoung et al., 2020). Accordingly, building timely seasonal forecasts of dam inflow is essential for anticipatory reservoir planning. To tackle this challenge, a range of data-driven techniques, such as stochastic time series models and hybrid artificial intelligence models, have been developed to integrate climate information and improve the predictability of seasonal and intra-annual dam inflows (Ionita et al., 2008; Slater et al., 2023; Yuan et al., 2015).

Uncertainty remains a fundamental challenge in streamflow forecasting, and stochastic time series models, such as the auto-regressive integrated moving average (ARIMA) model, have been widely used and shown to be effective in this domain (Wagena et al., 2020). However, traditional time series models were initially designed to capture fundamental data patterns, often neglecting the variability of data (volatility). The incorporation of volatility into time series modeling, inspired by successful practices in financial modeling, frequently involves the application of stochastic volatility frameworks (Wang et al., 2020).

* Corresponding author.
E-mail address: hkwon@uos.ac.kr (H.-H. Kwon).

https://doi.org/10.1016/j.jhydrol.2026.136255
Received 20 January 2024; Received in revised form 5 January 2026; Accepted 14 August 2026
Available online 16 August 2026

This modeling paradigm originates from econometrics research on heteroscedasticity (i.e., non-constant variability) and has led to the development of autoregressive conditional heteroscedasticity (ARCH) models, where the conditional variance is modeled as a function of past disturbances (Engle, 1982). This was followed by the generalized ARCH (GARCH) framework and its further extensions (Bollerslev, 1986; Wang et al., 2020). In contrast to ARCH-type models, stochastic volatility (SV) models treat variance as an unobserved latent process (i.e., inferred from the observed data through statistical estimation) that evolves stochastically over time, offering greater flexibility in representing persistent and irregular variance dynamics (Harvey et al., 1994). Explicitly accounting for this conditional heteroscedasticity has great implications for hydrological modeling, where variability is inherently nonstationary, leading to enhanced robustness and reliability of probabilistic hydrological predictions (Wang et al., 2023; Zeng et al., 2022; Zha et al., 2020).

Regarding empirical (data-driven) models, particularly autoregressive time-series models, recognizing their limitations in representing complex hydrologic processes and catchment dynamics is crucial (Shabri and Suhartono, 2012; Valipour et al., 2013; Zhou et al., 2021). Recent advancements in hydrological modeling emphasize the need for robust inflow prediction models that fully consider the intricate interactions between hydrological and climate data (Lee et al., 2019b; Lima and Lall, 2010), with forecasting research emphasizing the integration of large-scale climate information with regional hydrometeorological data (Gong et al., 2010).

This integration seeks to clarify how large-scale climate anomalies influence regional hydrometeorological variables (e.g., streamflow, precipitation, and temperature), thereby improving process understanding and supporting risk assessments of extremes (Kwon et al., 2009a). Incorporating large-scale climate state variables (e.g., SST and SLP) into streamflow forecasting models provides the broader climate context that influences precipitation variability and subsequent runoff responses (Lima and Lall, 2010; Wei and Watkins, 2011). These linkages are commonly expressed through climate teleconnections, which transmit ocean–atmosphere anomalies across regions and influence hydroclimatic variability and extreme worldwide (Forootan et al., 2019).

These climate-hydrology linkages are globally relevant because large-scale modes of climate variability, such as El Niño Southern Oscillation (ENSO), and other ocean–atmosphere oscillations, modulate precipitation and streamflow patterns across many regions (Guo et al., 2021). The strength and expression of teleconnections vary by region depending on proximity to oscillation centers, atmospheric circulation pathways (i.e., particularly Rossby wave propagation), and regional hydrological characteristics, as SST anomalies can generate planetary-wave responses that preferentially affect specific regions (Li et al., 2025; Liu and Alexander, 2007).

For example, ENSO-related indices have been shown to influence river discharge across temperate and tropical regions, including North American river systems (Amarasekera et al., 1997; Chiew and McMahon, 2002; Ionita and Nagavciuc, 2020). In North America, studies have identified ENSO and the Pacific Decadal Oscillation (PDO) as primary drivers of streamflow variability and have reported forecast skill at seasonal lead times (e.g., 3–6 months) for basins such as the northwestern Columbia rivers and Upper Colorado basins (Lettenmaier, 1999; Hidalgo and Dracup, 2003; Singh et al., 2021; Tamaddun et al., 2017). In Europe, both ENSO and North Atlantic Oscillation (NAO) have been linked to streamflow variability, with significant winter NAO correlations reported for northwestern to central Europe (Ionita et al., 2008; Rimbu et al., 2004; Rust et al., 2021). Similarly, the PDO (associated with North Pacific SSTs) and the NAO (linked to large-scale SST and atmospheric circulation patterns) exert significant influence on precipitation and streamflow variability in East Asia (Lee et al., 2020; Ma et al., 2025).

In monsoon-dominated regions such as East Asia and South Asia, these teleconnections are especially challenging because the seasonal water cycle is highly concentrated and influenced by large-scale climate anomalies that affect monsoon timing and intensity (Han, 2019; Ma et al., 2025). In East Asia, the summer monsoon system is governed by the combined influence of the East Asian Summer Monsoon (EASM) and the western North Pacific subtropical high, resulting in strong seasonality and high interannual variability in precipitation (Choi and Ahn, 2019). The complex interactions between large-scale drivers and regional monsoon systems make skillful pre-season predictions particularly challenging in these basins, relative to regions where dominant modes of climate variability exhibit stronger and more temporally persistent control over precipitation and streamflow relationships (Hobeichi, 2024).

Studies within South Korea, such as those by Kim et al. (2020a,b) ad Kwon et al. (2008), have established links between climate teleconnections and extreme precipitation. Furthermore, Kim et al. (2022) focused on significant climate indices and their application to extreme precipitation modeling, while (Jung and Kim, 2022) improved predictive temperature and precipitation models by considering El Niño and La Niña. Large-scale climate state variables, including the North Atlantic Winter SST (Myoung et al., 2020) and Tropical Atlantic SST (Ham et al., 2017b), greatly influence precipitation variability in South Korea.

In the context of streamflow prediction, studies from Lee et al. (2020) and Lee et al. (2019a) explored the potential role of climate predictors, including SST and Sea Level Pressure (SLP), on a reservoir inflow forecasting model. Kim et al. (2012) investigated typhoon- and non-typhoon-induced streamflow volume, shedding light on regional hydrological impacts. In another study, Lee et al. (2020) presented monthly inflow forecasting using teleconnection, demonstrating the potential for a reservoir operation strategy for droughts. Moreover, highlighting the importance of large-scale climate indices as drivers for streamflow in South Korea, Han et al. (2023) developed a Long Short-Term Memory (LSTM) deep learning model for monthly dam inflow prediction. Additionally, research has investigated pre-season North Atlantic SST (Choi and Ahn, 2019; Noh and Ahn, 2022; Zheng et al., 2016) as a reliable climate predictor for the East Asian summer monsoon.

Bayesian modeling has significantly advanced uncertainty quantification and parameter estimation in hydrology (Smith and Marshall, 2008). By integrating prior knowledge with observations, Bayesian frameworks enable probabilistic inference that explicitly represents uncertainty in both model parameters and predictions. This probabilistic formulation is particularly suitable for seasonal forecasting because decision-making benefits from predictive distribution (credible intervals) rather than single deterministic estimates. In streamflow forecasting, autoregressive models such as ARIMA have been widely used, and extensions incorporating exogenous inputs (ARIMAX) have been applied to improve predictive skill by integrating climate or hydrometeorological information (Islam and Imteaz, 2020; Pektaş and Kerem Cigizoglu, 2013).

In this study, we develop a Bayesian autoregressive (AR) forecasting model to predict one-season-ahead dam inflow. Large-scale, slow-onset climate circulations are incorporated as exogenous predictors (ARX) to capture teleconnection-driven variability and enhance predictive skill beyond memory-based autoregressive processes with interpretability of climate-streamflow linkages. In addition, we explicitly model time-varying variance through a stochastic volatility structure (ARXSV), allowing the framework to account for heteroskedastic behavior commonly observed in hydroclimatic time series.

Soyang Dam, the largest multipurpose dam in South Korea, serves as the focal point for this research due to its high inflow variability and its role in supplying water to approximately 40% of the national population. To provide operational context for reservoir management during drought events, we qualitatively compared our proposed statistical forecasting framework with streamflow scenarios derived from a dynamical seasonal forecasting system (GloSea5).

Accordingly, this study addresses two research questions: (1) Can pre-season large-scale climate variables provide skillful season-ahead forecasts of summer (JJA) streamflow in a monsoon-dominated basin? And (2) Can these probabilistic forecasts be used to anticipate hydrological drought states and extremes in a way that is informative for reservoir operations and transferable to other basins facing similar hydroclimatic challenges? Our modeling framework explicitly separates (i) memory-based persistence, (ii) exogenous climate drivers, and (iii) time-varying uncertainty (stochastic volatility). It can be readily adapted to other basins exhibiting strong seasonality and non-stationary variance.

In practice, extending the framework to a new basin primarily involves (a) selecting regionally relevant seasonal climate predictors (e.g., large-scale teleconnection indices) and (b) re-estimating the ARXSV parameters using local streamflow records, after which probabilistic season-ahead forecasts and drought indices can be produced within the same workflow. As such, our framework offers broader utility for supporting season-ahead water-resources decision-making, especially during critical periods such as the summer monsoon season.

2. Basin and methods

2.1. Soyang Dam basin

With a capacity to hold 2.9 billion tons of water and a drainage area of 2703 km^2, Soyang Dam is the largest in South Korea, and it has one of the nation's longest hydrometeorological records to date, spanning almost 50 years (1974–2023) (Fig. 1). The prolonged high temperatures and extreme precipitation events brought on by climate change have an impact on Soyang Dam's water resources management, with an increase of variability in inflow that needs to be properly considered to provide a better management plan for flood control, water supply, and power generation in the metropolitan area (Hong et al., 2020; Lee and Kim, 2021). In 2015, South Korea experienced a persistent shortage of precipitation, with the overall annual precipitation being only half of the historical average. This led to a critically low water level in the Soyang River's multi-purpose dam, reaching the second-lowest recorded level since 1978, causing the reservoir to nearly run dry due to reduced inflow (Hong et al., 2016). This study focused on the Soyang River's multi-purpose dam as a study area due to its importance and role in water supply for domestic, industrial, and irrigation use, especially for the capital area of Seoul in South Korea.

2.2. Inflow data and climate state variables

Daily dam inflow data spanning 44 years (1979–2022) were obtained from the Water Management Information System (WAMIS) via (https://www.wamis.go.kr). South Korea experiences around 60–70% of its annual rainfall between June and September (Han et al., 2023). Interestingly, there is a decreasing trend in streamflow despite an overall increase in annual precipitation within this watershed (Kang et al., 2017). This pattern suggests changes in runoff generation that may be linked to soil moisture dynamics under climate change. More importantly, rising temperatures can increase atmospheric evaporative demand (potential evapotranspiration), which accelerates soil-moisture depletion and may reduce runoff efficiency even if precipitation increases (Hong et al., 2020; Koralegedara et al., 2025). Rainfall during the monsoon and wet seasons has a large implication on water resources management. In this context, a lack of precipitation at these times may cause water shortages over the following years (Jung et al., 2011).

Extreme rainfall in the Soyang Dam watershed, often associated with monsoon depressions and typhoons in South Korea, typically occurs in late summer, spanning from mid-July to the end of August. Therefore, for the purpose of our research, we focused on the seasonal inflow during the summer monsoon JJA (Fig. 2). To characterize temporal dependence in streamflow across time scales (monthly, seasonal, and annual JJA means), we examined autocorrelation (ACF) and partial autocorrelation (PACF) functions (Fig. 3). The ACF reflects total

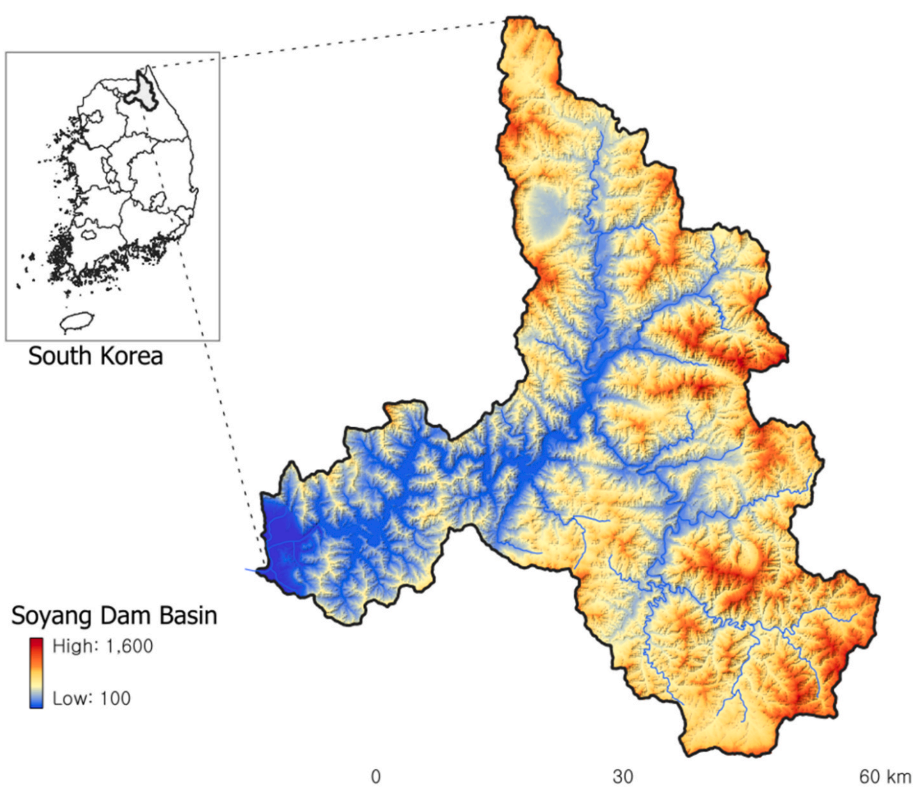

Fig. 1. Location of the Soyang Dam basin and its topology in South Korea.

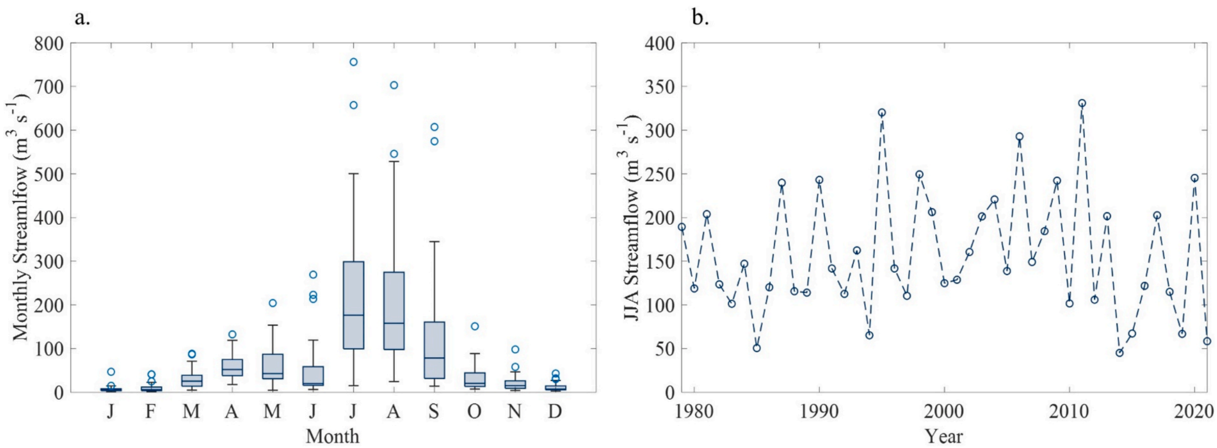

Fig. 2. Hydrological information: (a) monthly streamflow box plot and (b) annual JJA streamflow.

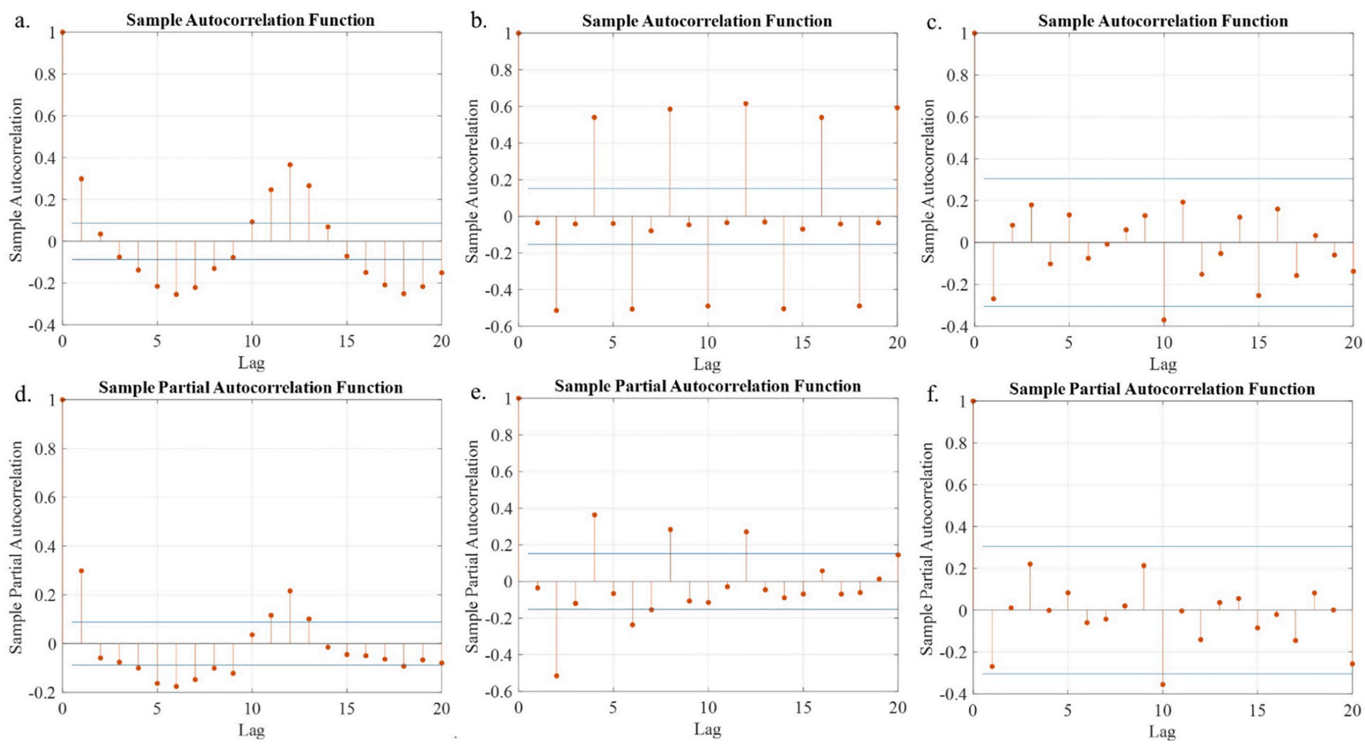

Fig. 3. Autocorrelation function (ACF) and partial autocorrelation function (PACF) of streamflow at different aggregation scales: (a,d) monthly, (b,e) seasonal, and (c,f) annual JJA. The blue horizontal lines represent approximate 95% confidence bounds for testing the significance of (partial) autocorrelations (null: no autocorrelation). (For interpretation of the references to colour in this figure legend, the reader is referred to the web version of this article.)

correlation across lags, whereas the PACF isolates the direct correlation at a given lag after removing the influence of shorter lags. Autocorrelation (and partial autocorrelation) values exceeding the blue bounds are considered statistically significant at the 5% level (null: zero autocorrelation). At the monthly scale, the PACF is strongest at lag 1 and then gradually decays, indicating short-term persistence and pronounced seasonality. At the seasonal scale, significant correlations persist at intermittent lags, including lag 2 (JJA at year t vs. DJF at year t) and lag 4 (JJA at year t vs. JJA at year t − 1), suggesting seasonal memory. In contrast, for annual JJA streamflow (Fig. 3c, f), dependence weakens substantially, indicating limited interannual persistence in summer inflow.

Given this weak year-to-year persistence, we further investigated the relationship between JJA inflow variability and large-scale climate variables (or predictors) in the preceding spring to explain variability beyond autoregressive dependence. This study employed climate state variables such as Sea Surface Temperature (SST) from HadISST with spatial resolution 1° reconstruction provided by the Met Office Hadley Centre (https://www.metoffice.gov.uk/) and Sea Level Pressure (SLP) from NCEP/NCAR reanalysis data (https://psl.noaa.gov/) with a resolution of 2.5°.

2.3. Droughts and dam operation

To ensure the predictability of the statistical model developed in this study and to provide valuable insights for dam operation related to dam inflow, this study conducted a comparative analysis between a statistical modeling approach and a dynamic modeling framework. Here, the statistical ARXSV framework provides a one-season-ahead forecast of target JJA inflow using pre-season (spring) climate predictors. By contrast, the GloSea5–ABCD outputs are used as seasonal dynamical simulations for the target JJA period (available from 2016 onward) and are included for qualitative operational context, rather than as lead-time-matched forecasts for quantitative skill benchmarking. More specifically, we utilized output from the Met Office/KMA seasonal forecasting model and the Global Seasonal Forecast System version 5 (GloSea5) for the dynamic modeling aspect. The precipitation and temperature from the GloSea5 are then fed into a rainfall-runoff model to simulate ensemble streamflow scenarios. The GloSea5 data were obtained from the KMA, and a conceptual ABCD rainfall-runoff model (Kwon et al., 2020) was employed for analysis. This comparative study aims to enhance our understanding of modeling approaches for informed dam inflow management.

Furthermore, this study offers a predicted hydrological drought index informed by streamflow forecasting. The concept of hydrological drought is typically linked to deficits, especially in water storage, which is directly associated with insufficient streamflow. In this regard, the Standardized Streamflow Index (SSI) can be effectively used to assess the hydrological drought. The SSI, analogous in computation to the Standardized Precipitation Index (SPI) (McKee et al., 1993), relies on the cumulative probability of streamflow calculated over various accumulation periods (e.g., 1, 3, 6, and 12 months). In this study, SSI is derived from the ARXSV season-ahead inflow forecasts and compared against SSI computed from the corresponding GloSea5–ABCD JJA simulations for qualitative interpretation. The predicted streamflow in this study was then transformed into the SSI and analyzed as seasonal simulations of the JJA period to better identify the occurrence of extremes, particularly droughts in the Soyang Dam watershed. A negative value of the index indicates drier than average conditions, while a positive value indicates wetter than average conditions. For the complete flowchart of the methodology used in this research, please refer to (Fig. 4).

3. Predictor selection

The East Asian Summer Monsoon (EASM) is a regional climate system in East Asia that brings heavy precipitation to the East Asia region, where its variability poses challenges for streamflow prediction due to

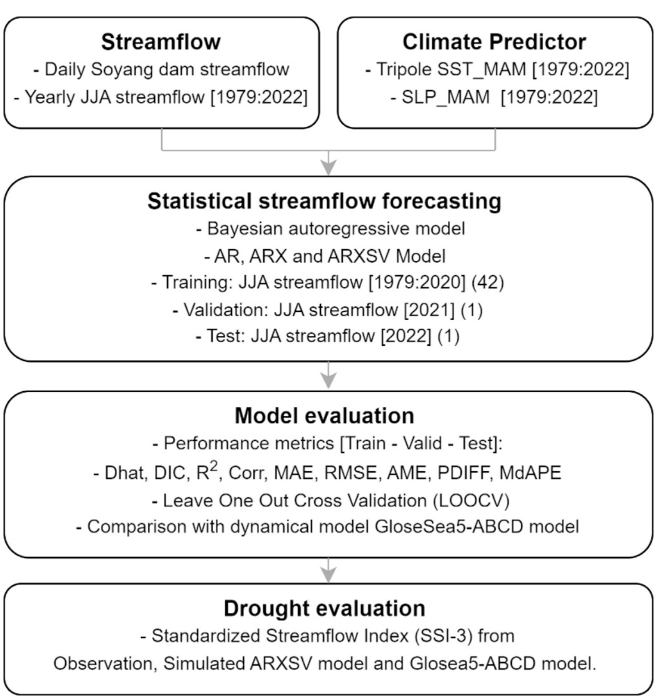

Fig. 4. Flowchart of the climate-informed streamflow modeling and validation procedure.

the occurrence of large-scale catastrophic events like floods and droughts. EASM is influenced by various large-scale climate patterns, including but not limited to the ENSO, North Atlantic Oscillation (NAO), and PDO. The EASM is typically associated with a strengthened western North Pacific subtropical high, leading to increased rainfall along the subtropical monsoon front during the boreal summer. On the other hand, a weak EASM is generally accompanied by a weakened western North Pacific subtropical high, resulting in deficient rainfall in the same region (Baek et al., 2017; Seo et al., 2012). In South Korea, the EASM, known as Changma, leads to heavy precipitation between July and August, with around 60% of the annual rainfall concentrated in the rainy summer season (Lee et al., 2017). Therefore, accounting for the distinct precipitation patterns during the EASM is crucial for effective water resources management. Myoung (2021) found a significant trend of cold winters followed by hot summers in South Korea due to the combined effects of the warm springtime SST in the western tropical Pacific and North Atlantic.

In particular, the relationship between the Atlantic SLP and SST has been documented. On one side, the relationship between the NAO during the boreal spring and the EASM during the following boreal summer has been investigated (Choi and Ahn, 2019; Deng et al., 2019; Sung et al., 2006; Wu et al., 2009; Zheng et al., 2016; Zuo et al., 2013). The NAO is known to lead to unusual Rossby wave trains over the North Atlantic and Eurasia by changing the baroclinic instability in the North Atlantic (Deng et al., 2019).

Previous research has observed evidence through numerical experiments that spring NAO can trigger a tripole SST pattern in the North Atlantic that can persist until summer and exert an effect on the EASM (Wu et al., 2012; Wu et al., 2009; Zheng et al., 2016; Zuo et al., 2013). This implies that the relationship between the NAO and the EASM can be interpreted as a strong correlation between the North Atlantic (NA) SST and the EASM (Choi and Ahn, 2019; Ham et al., 2017a). The connection of Tropical Atlantic SST (Choi and Ahn, 2019; Ham et al., 2017a) and tripole SST (Deng et al., 2019; Myoung, 2021) with EASM has also been reported. The influence of summer NAO on the spring NAO-based predictability for EASM has also been demonstrated (Zheng et al., 2016). In addition, there is evidence suggesting a relationship between North Atlantic SST anomalies and precipitation patterns in South Korea (Noh and Ahn, 2022). Notably, findings have revealed that variations in early winter precipitation are associated with spring SST patterns in the North Atlantic Ocean at a substantial lead time of greater than six months. Furthermore, a significant correlation was found between Korean precipitation anomalies and the tropical Atlantic SST during the JJA season for the 1979–2010 period (Ham et al., 2017a,b). The impact of the NA SST on the EASM was significantly increased after the 2000s (Lee et al., 2017).

In the context of streamflow forecasting, the use of North Atlantic SST has been reported (Lee et al., 2020). Previous literature has only considered North Atlantic SST by relating it to East Asian summer (or winter) monsoons and rainfall anomalies in South Korea. In these contexts, teleconnections associated with SST and SLP can provide direct implications for streamflow patterns as predictors for streamflow modeling or forecasting. While previous research related to East Asia or South Korea has established these correlations, their impact on streamflow patterns remains unexplored, representing a key objective of this research. Understanding the relationships between North Atlantic SSTs, SLPs, and streamflow patterns can provide valuable insights for streamflow modeling and forecasting.

One primary focus of this study is to further explore the influence of teleconnections in the North Atlantic region on the Soyang Dam inflow. The correlation maps between the Soyang Dam inflow from JJA with SST and SLP indices for the concurrent season (i.e., JJA) and the two preceding seasons, i.e., MAM and DJF, are presented in Fig. 5. The JJA streamflow is more noticeably correlated with SST and SLP during the MAM spring season. Previous studies have shown that tripole-like teleconnections can be used to implicate information of the North Atlantic,

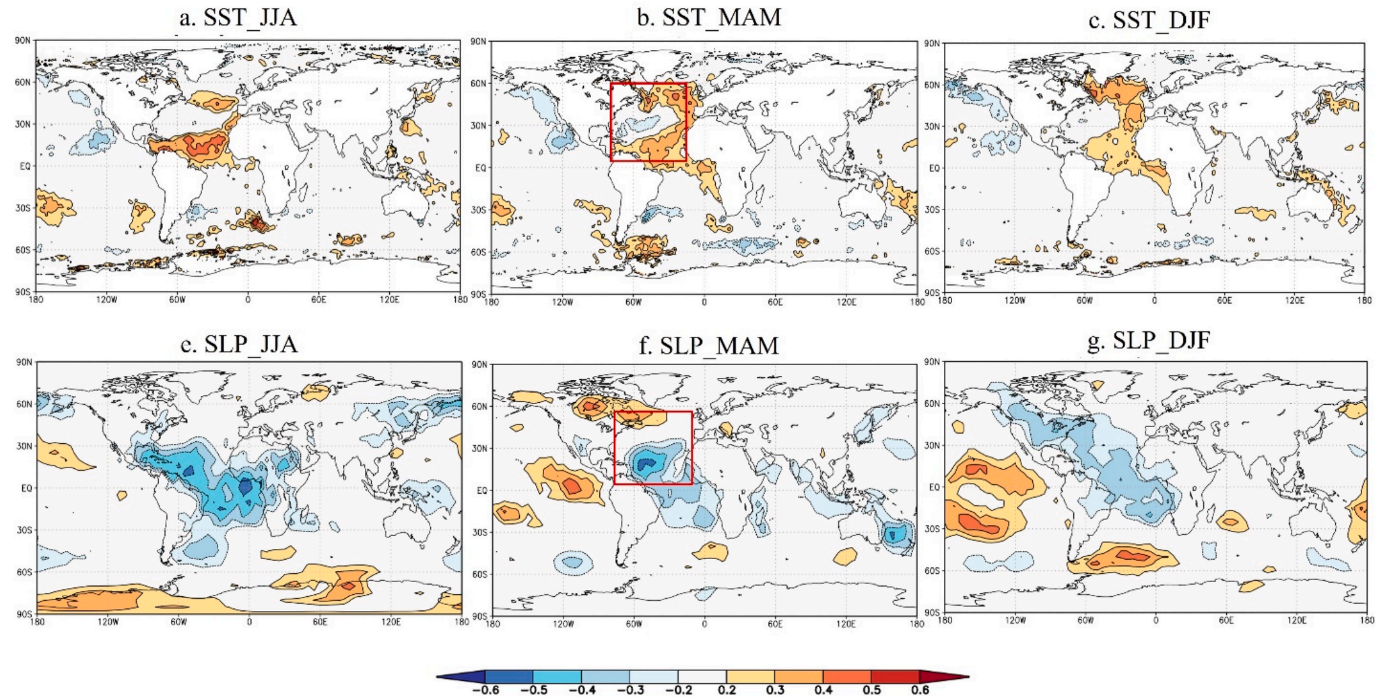

Fig. 5. Correlation map of the Soyang Dam June to August streamflow (JJA). (a) – (c) SST indices and (d) – (f) SLP indices at the concurrent, lagged 3-month, and lagged 6-month conditions from 1979 to 2022. The March to May (MAM) correlations in the North Atlantic area under study for SST and SLP are highlighted with red boxes. (For interpretation of the references to colour in this figure legend, the reader is referred to the web version of this article.)

as shown by Myoung (2021). That study also showed that South Korea has experienced a recent pattern of cold winters followed by hot summers, attributed to the combined influence of warm conditions in the western tropical Pacific and anomalies in the North Atlantic during the spring season. Consequently, the relationship between JJA and DJF was also observed in light of these trends. The tripole-like teleconnection was identified, with areas having positive correlations (shown in red) or negative correlations (shown in blue) between climate state variables (i.e., SST and SLP) and streamflow for the JJA and DJF seasons (Fig. 6).

The SST index was defined by selecting specific regions over the North Atlantic Ocean that exhibit strong associations with JJA streamflow patterns (Table 1). The tripole SST index was computed by including SST_A, SST_B, and SST_C from selected zones, as adopted from the methodology of Myoung (2021). After applying the $SST_A - SST_B, + SST_C$ (SST tripole), the correlation coefficient is about 0.42, suggesting a moderate positive correlation (*p-value* = 0.0054). On the other hand, the correlation coefficient between SLP_MAM and JJA inflow is about −0.51 (*p-value* = 0.00042). The p-values indicate that the observed correlation is statistically significant at the 0.05 significance level. Scatter plots between the spatial averages of SST tripole and SLP with seasonal JJA streamflow for 1979 to 2022 are illustrated in Fig. 7.

4. Statistical streamflow forecasting model

Uncertainty is a prevalent issue stemming from different sources, including data incompleteness, natural variability, and incomplete process representation. Here, we adopt a Bayesian modeling-based stochastic framework for season-ahead streamflow forecasting using large-scale climate predictors, enabling explicit quantification of uncertainty in parameter estimation and predictive distributions. Our objective is to develop and evaluate climate-informed autoregressive models and, in particular, to examine a stochastic-volatility formulation in which the conditional variance evolves as an autoregressive process. This allows the model to represent time-varying variability through a latent (unobserved) volatility process inferred from the observed streamflow series, thereby improving finite-sample inference and probabilistic forecasts.

We consider three models of increasing complexity: (1) a baseline autoregressive model (AR), (2) an autoregressive model with exogenous climate predictors (ARX), and (3) an ARX model coupled with stochastic volatility (ARXSV) to capture time-varying uncertainty. All models are estimated within a unified Bayesian framework. A full Bayesian model is defined by the joint prior distribution of parameters Θ and the likelihood $p(\mathbf{Y}|\Theta)$, yielding the posterior distribution $p(\Theta|\mathbf{Y})$ via Bayes' theorem (Eq. (1) (Meyer, 2000)). We model log-transformed streamflow in all autoregressive formulations and estimate parameters using Markov Chain Monte Carlo (MCMC) sampling implemented in Bayesian inference using Gibbs sampling (BUGS). We ran three independent chains with 5,000 iterations discarded as burn-in and retained 2,000 samples per chain, yielding 6,000 posterior samples in total. The dependence structure of the hierarchical model is summarized using a directed acyclic graph (Fig. 8).

$$p(\Theta|\mathbf{Y}) = \frac{p(\Theta, \mathbf{Y})}{p(\mathbf{Y})} = \frac{p(\Theta)p(\mathbf{Y}|\Theta)}{p(\mathbf{Y})} \tag{1}$$

where the posterior distribution $p(\Theta|\mathbf{Y})$ is expressed as the product of the prior distribution $p(\Theta)$ and the likelihood $p(\mathbf{Y}|\Theta)$.

Prior specifications follow weakly non-informative (diffuse) distributions to allow data to dominate inference (Meyer and Yu, 2000). Variance (precision) parameters are assigned Gamma priors to enforce positivity, consistent with standard BUGS practice for Bayesian time-series and stochastic volatility models. The three models share a common autoregressive baseline but differ in parameter sets: AR ($\boldsymbol{\alpha}, \sigma^{AR}$),), ARX ($\boldsymbol{\beta}, \sigma^{X}$), and ARXSV ($\boldsymbol{\gamma}, \boldsymbol{\delta}, \tau^{SV}$). Model performance is assessed in Section 4.4 using leave-one-out cross-validation (LOOCV) based on posterior predictive summaries, and overall Bayesian model adequacy is evaluated using deviance-based criteria (DIC). For LOOCV-based skill metrics, we used the posterior predictive median as the point estimate for each held-out year, while uncertainty was summarized using credible intervals.

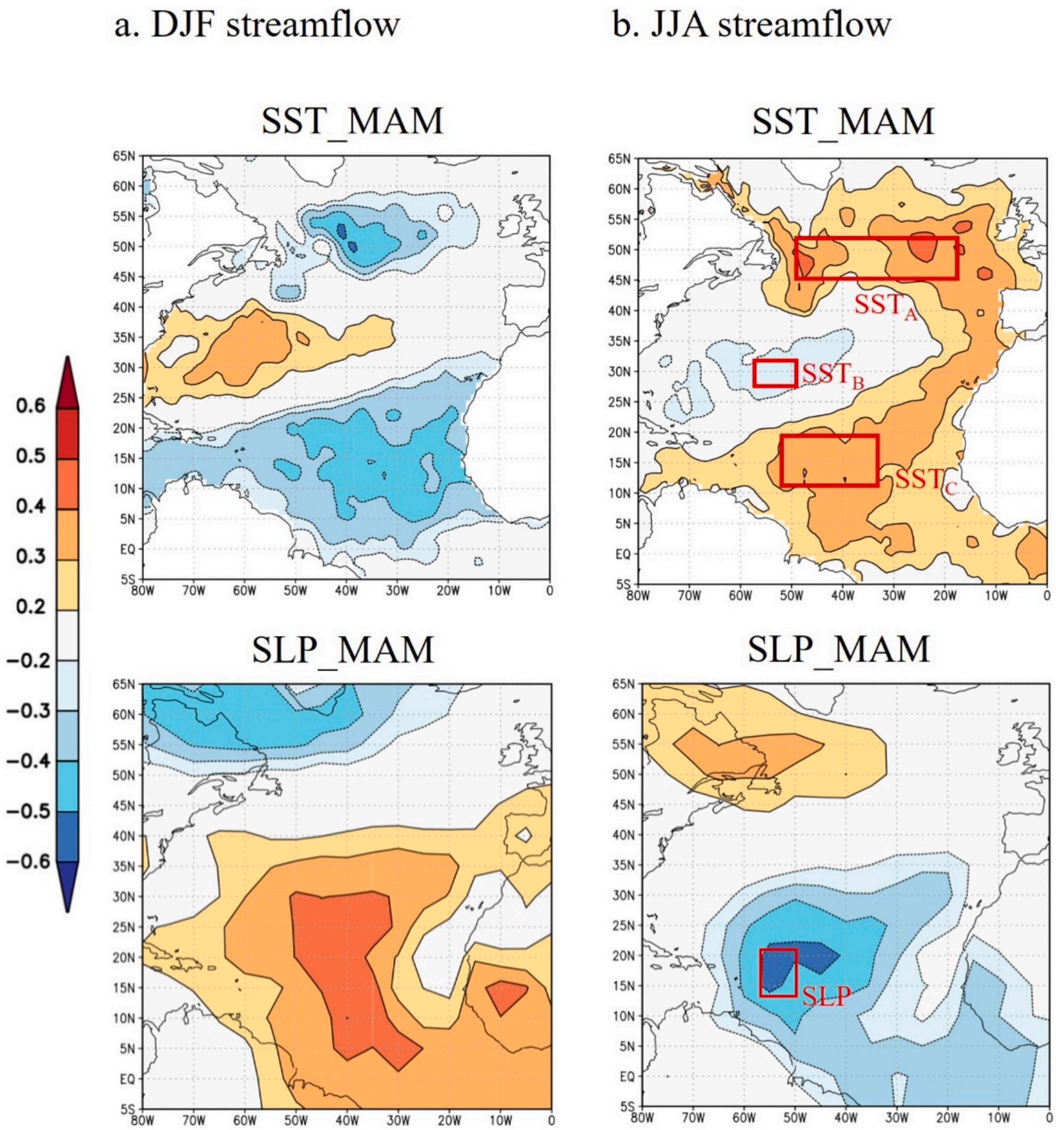

Fig. 6. Correlation map of SST_MAM with (a) Soyang Dam DJF streamflow from 1979 to 2021 lagged at 9 months and (b) Soyang Dam JJA streamflow from 1979 to 2022 lagged at 3 months. The selected spring (MAM) North Atlantic climate teleconnections in relation to the JJA streamflow are shown by red boxes, including SST_A, SST_B, SST_C, and SLP. (For interpretation of the references to colour in this figure legend, the reader is referred to the web version of this article.)

Table 1
Sea surface temperature and sea level pressure (SST, SLP) from the spatial average of selected zones in the North Atlantic region and their correlation with seasonal JJA streamflow for 1979 to 2022.

Predictors	Selected Zone	Correlation
SST Tripole	[SST_A – SST_B + SST_C]	0.42
SST_A	46° N – 52° N, 20° W – 50° W	0.41
SST_B	28° N – 32° N, 60° W – 48° W	–0.37
SST_C	12° N – 19° N, 52° W – 34° W	0.33
SLP	16° N – 21° N, 52° W – 56° W	–0.51

Significant at 95% confidence level.

4.1. Autoregressive (AR) model

The autoregressive (AR) model is one of the most used time series models in the field of hydrology. An AR(p) model of order p is defined as follows:

$$Y_t^{AR}\ Normal\left(\mu_t^{AR}, \sigma^{AR}\right) \tag{2}$$

$$\mu_t^{AR} = \alpha_1 Y_{t-1} + \alpha_2 Y_{t-2}, \cdots, \alpha_p Y_{t-p} \tag{3}$$

$$\sigma^{AR}\ Gamma\ (0.1\ ,\ 0.1) \tag{4}$$

$$\boldsymbol{\alpha_p}\ Normal\ (0.1\ ,\ 0.1) \tag{5}$$

where Y_t^{AR} represents the natural logarithm of the JJA streamflow at year t. The μ_t^{AR} and σ^{AR} represent the location and scale parameters (i.e., mean and variance) of the normal distribution, respectively, while $\boldsymbol{\alpha_p}$ represents the autoregressive parameters. A diffuse Gamma prior is assigned to the variance-related scale parameter (σ^{AR}) to ensure positive support and to limit prior influence on posterior estimates, whereas Normal priors are used for the autoregressive parameters (α_p) to provide symmetric, weakly informative regularization around zero. In the BUGS parameterization, the second argument of the Normal distribution is the precision (inverse variance), and the Gamma distribution is specified by shape and rate; we set these hyperparameters to be weakly informative so that the data dominate posterior inference while respecting parameter constraints. The autoregressive order of Y_t^{AR} (JJA streamflow) was determined to be one through the use of the Yule-Walker method and the

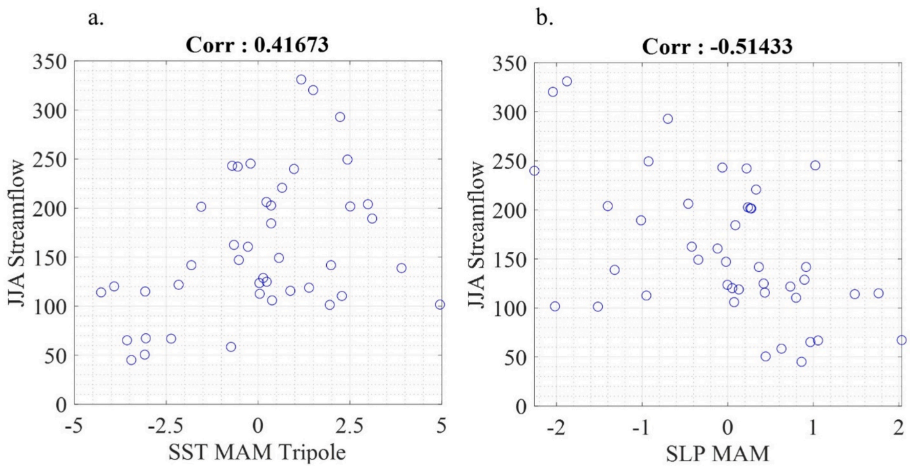

Fig. 7. Scatter plots between the spatial averages of (a) SST tripole and (b) SLP with seasonal JJA streamflow for 1979 to 2022.

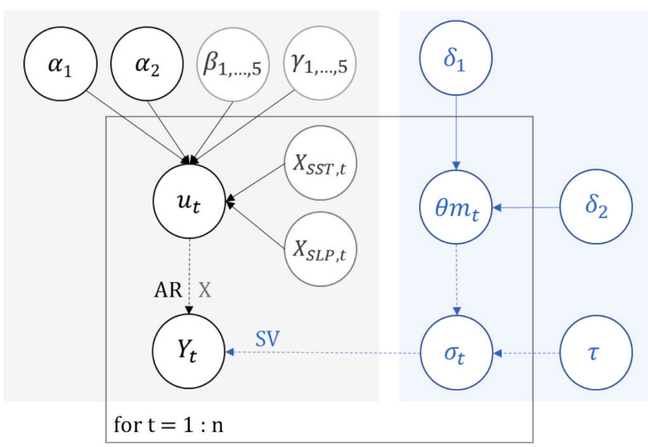

Fig. 8. The dependence properties between variables are specified using a directed acyclic graph (DAG), explicitly showing the conditional relationships. Dashed arrows indicate stochastic dependence, while solid arrows indicate logical functions. The loop in the model is enclosed on a plate for a given time (t).

partial auto-correlation function (Fig. 3).

4.2. Autoregressive exogenous (ARX) model

The autoregressive exogenous (ARX) model extends the conventional AR model by incorporating exogenous (X) variables to account for the influence of external climate factors, as in this research. An autoregressive exogenous AR(p) X model is defined by replacing Eq. (2) with Eq. (6) under the same likelihood function adopted in the AR model (Eq. (1)), as follows:

$$Y_t^X \; Normal\left(\mu_t^X, \sigma^X\right) \tag{6}$$

$$\mu_t^X = \beta_1 + \beta_2 Y_{t-1} + \beta_3 X_{SST,t} + \beta_4 {X_{SST,t}}^2 + \beta_5 X_{SLP,t} \tag{7}$$

$$\sigma^X \; \text{Gamma} \; (0.1 \; , \; 0.1) \tag{8}$$

$$\boldsymbol{\beta}_{1,2,\dots,5} \; Normal \; (0.1 \; , \; 0.1) \tag{9}$$

where Y_t^X represents the natural logarithm of the JJA streamflow at year *t*. Additionally, X_{SST} and X_{SLP} represent the climate predictors defined as the spring tripole SST and spring SLP, which are defined in Table 1. A diffuse gamma prior is used for the variance-related parameter (σ^X) to ensure positivity, and Normal priors are assigned to the regression coefficients $\boldsymbol{\beta}_{1,2,\dots,5}$ as weakly informative symmetric specifications.

4.3. Stochastic volatility (ARXSV) model

Stochastic approaches have been shown to be highly helpful for hydrological variables where uncertainty needs to be considered (Kwon et al., 2009b). The ARXSV, i.e., the Bayesian model with stochastic volatility, combines Bayesian inference and the concept of stochastic volatility. Hierarchical Bayesian inference was employed to estimate the posterior distribution of the independent variables in the ARX model. Within this modeling framework, volatility (representing the degree of variation or fluctuation) is considered a latent variable that can vary over time. Unlike conventional autoregressive models, this approach acknowledges that volatility can exhibit random fluctuations and temporal changes, providing a more realistic representation of the data. The Bayesian Stochastic Volatility (SV) model is defined as:

$$Y_t^{SV} \; Normal\left(\mu_t^{SV}, \sigma_t^{SV}\right) \tag{10}$$

$$\mu_t^{SV} = \gamma_1 + \gamma_2 Y_{t-1} + \gamma_3 X_{SST,t} + \gamma_4 {X_{SST,t}}^2 + \gamma_5 X_{SLP,t} \tag{11}$$

$$\sigma_t^{SV} = \exp\left(\theta_t^{SV}\right) \tag{12}$$

$$\theta_t^{SV} \; Normal \; \left(\theta m_t^{SV} \; , \; \tau^{SV}\right) \tag{13}$$

$$\theta m_t^{SV} = \delta_1 + \delta_2\left(\theta m_{t-1}^{SV} - \delta_1\right) \tag{14}$$

$$\tau^{SV} \; Gamma \; (0.1 \; , \; 0.1) \tag{15}$$

$$\boldsymbol{\gamma}_{1,2,\dots,5} \; Normal \; (0.1 \; , \; 0.1) \tag{16}$$

$$\delta_1 \; Normal \; (0.1 \; , \; 0.1) \tag{17}$$

$$\delta_2 \; Normal \; (1, 0.1) \tag{18}$$

where σ_t^{SV} is the scale parameter as a function of time (t) of the Y_t^{SV}(the natural logarithm of the JJA streamflow). The time-varying scale parameter σ_t^{SV} is alternatively informed by θ_t^{SV}, assuming a normal distribution with mean θm_t^{SV} and variance τ^{SV}. The mean θm_t^{SV} is subsequently described by a lag-1 autoregressive process, as written in Eq. (14), and a diffuse gamma distribution is used for the variance (τ^{SV}), as shown in Eq. (15). Normal prior distributions are used for the regression parameters $\boldsymbol{\gamma}_{1,2,\dots,5}$ and $\boldsymbol{\delta}_{1,2}$ for mean and variance parameters, respectively. The stochastic volatility component follows the BUGS implementation framework of Meyer and Yu (2000), with priors calibrated for efficient MCMC sampling in BUGS.

Overall, these models and their associated priors are presented to demonstrate the methodology used in this research, which involves statistical modeling and Bayesian inference for streamflow forecasting. These models allow the incorporation of various factors, including exogenous climate variables and stochastic volatility, to enhance predictions and capture the underlying mechanisms of hydrometeorological variability.

4.4. Evaluation methods

To ensure model robustness, we employed a combination of Bayesian performance diagnostics and cross-validation techniques. Model performance and complexity were assessed using the average deviance Dhat ($\widehat{D}$) and the Deviance Information Criterion (DIC), which have proven to be efficient in evaluating Bayesian models (Berg et al., 2004). $\widehat{D}$ is defined as a point estimate of the deviance (i.e., lack of fit) obtained by substituting the posterior mean of the parameters $\overline{\theta}$ into the likelihood,

$$\widehat{D} = -2\log p(y|\overline{\theta}) \tag{19}$$

This metric directly reflects how well the posterior mean model explains the observed data and is therefore suitable for comparing probabilistic Bayesian models (Berg et al., 2004; Spiegelhalter, 2002). DIC complements $\widehat{D}$ by penalizing model complexity through the effective number of parameters p_D and is defined as

$$DIC = \widehat{D} + 2p_D \tag{20}$$

To complement these deviance-based diagnostics, we further applied a Leave-One-Out Cross-Validation (LOOCV) technique, which iteratively excludes one year for validation while using the remaining years for training. For each LOOCV fold, posterior predictive distributions were generated for the held-out year, and predictive skill was summarized using the coefficient of determination (R^2), correlation coefficient (Corr), mean absolute error (MAE), and root mean squared error (RMSE) (Dawson et al., 2007; Modarres and Ouarda, 2013; Wang et al., 2023), using posterior predictive median values as point summaries. Finally, within the LOOCV framework, the 2022 case was treated as the most recent out-of-sample fold (i.e., the year excluded for validation). The 2022 posterior predictive streamflow was then compared with the observed streamflow to illustrate the model's out-of-sample performance for the latest year.

5. Results and discussion

5.1. Autoregressive model performance

Next, we assessed the performance of various autoregressive models applied in this study: the (a) conventional autoregressive (AR), (b) autoregressive with exogenous variables (ARX), and (c) autoregressive exogenous with stochastic volatility (ARXSV) models. Our aim was to understand how these models performed in predicting JJA seasonal streamflow using autoregressive patterns and how they identified predictors derived from climate state variables. With the ARX and ARXSV models, we assessed the effects of inclusion of preceding season climate indices (as illustrated in Fig. 6). The ARX_1, ARX_2, and ARX models include the effects of the pre-season Atlantic Sea surface temperature (SST_MAM), sea level pressure (SLP_MAM), and the combined effects of the two anomalous climate patterns, respectively.

The summary of this autoregressive model performance can be found in Table 2. We obtained these results through a validation process involving a train-validation-test approach. The average deviance ($\widehat{D}$) served as a key measure of each model's goodness of fit, where a lower value indicates a better fit to the data. Notably, the tripole SST index (ARX_1) emerged as an influential factor among the large-scale climate signals, significantly reducing the deviance from 53.9 (AR) to 28.8 (ARX_1) when included as a predictor. Incorporating both SST and SLP climate information (ARX) further improved the model performance to a deviance of 26.1. Among all the variations, the combined stochastic volatility model (ARXSV) exhibited the lowest deviance $\widehat{D}$ of 1.7, indicating the closest fit to observed data. A visual comparison of these models is presented in (Fig. 9), which reveals the challenge of simulating the JJA streamflow trend with a stationary AR model without an exogenous predictor. However, the introduction of climate and volatility information notably enhanced the model's ability to capture these trends, demonstrating its use in streamflow predictions.

Table 2
Model performance of the autoregressive models.

Model	Performance metrics					
	$\widehat{D}$	DIC	R^2	Corr.	MAE	RMSE
AR	53.9	59.8	0.060	0.196	55.8	71.0
ARSV	34.8	60.6	0.435	0.277	54.6	67.8
ARX_1	28.8	38.8	0.102	0.686	42.7	52.6
ARX_2	42.7	50.8	0.352	0.551	46.7	59.8
ARX	26.1	38.2	0.533	0.730	40.3	49.1
ARXSV	1.7	35.1	0.571	0.756	35.2	47.9

To further assess the model performance, we employed the Deviance Information Criterion (DIC) to assess the balance of the goodness of fit and model complexity. Notably, a lower DIC implies a better balance. With this, the ARXSV model had the lowest DIC of 35.1, despite its increased complexity resulting from the added stochastic volatility factor. In contrast, the ARX model exhibited a higher DIC of 38.2. Although the ARX and ARXSV models yield similar posterior predictive medians in Fig. 9, the ARXSV model achieves lower $\widehat{D}$ and DIC, indicating an improved likelihood-based fit and better uncertainty representation through time-varying variance (stochastic volatility). This suggests that ARXSV better captures the probabilistic structure of the observations beyond mean behavior. Moreover, the ARXSV model resulted in a higher R-squared value of 0.571 and a strong correlation coefficient of 0.756, indicating that it explains a significant portion of the data variability and yields strong agreement between predicted and observed data, respectively. Furthermore, the ARXSV model also performed best in terms of the lowest mean absolute error (MAE) and root mean square error (RMSE), confirming its predictive accuracy.

The ARXSV model's strength lies in its ability to combine prior knowledge with data-driven insights through the successful integration of Bayesian inference and stochastic volatility. This not only quantifies the uncertainty of parameters in the model but also leverages prior latent volatility, enhancing the robustness and reliability of parameter estimates. Overall, the ARXSV model excelled in all performance metrics, demonstrating its improved ability to predict the JJA seasonal streamflow. This model shows promise for precise streamflow prediction and efficient water resource management because of its ability to model the variability of streamflow; this is especially true given South Korea's distinct hydrometeorological circumstances.

In Bayesian statistics, the credible interval or the Bayesian confidence interval provides a range of values for a parameter showing the likelihood of the true value of the estimated parameter based on the posterior distribution. The estimated model parameters with credible intervals are presented in Table 3. The kernel density estimates of the posterior distribution of the parameters, specifically in the autoregressive exogenous stochastic volatility (ARXSV) model, are shown in Fig. 10. These density estimates reveal the posterior mean and standard deviation of the parameters and illustrate the uncertainty distribution from the Bayesian inference. Significantly, the posterior mean and the credible intervals of the model parameters do not include zero (or only slightly include zero), as presented in (Fig. 10). This is a strong indicator of the parameters' statistical significance, implying low uncertainty and underscoring their importance in the model. Overall, the integration of

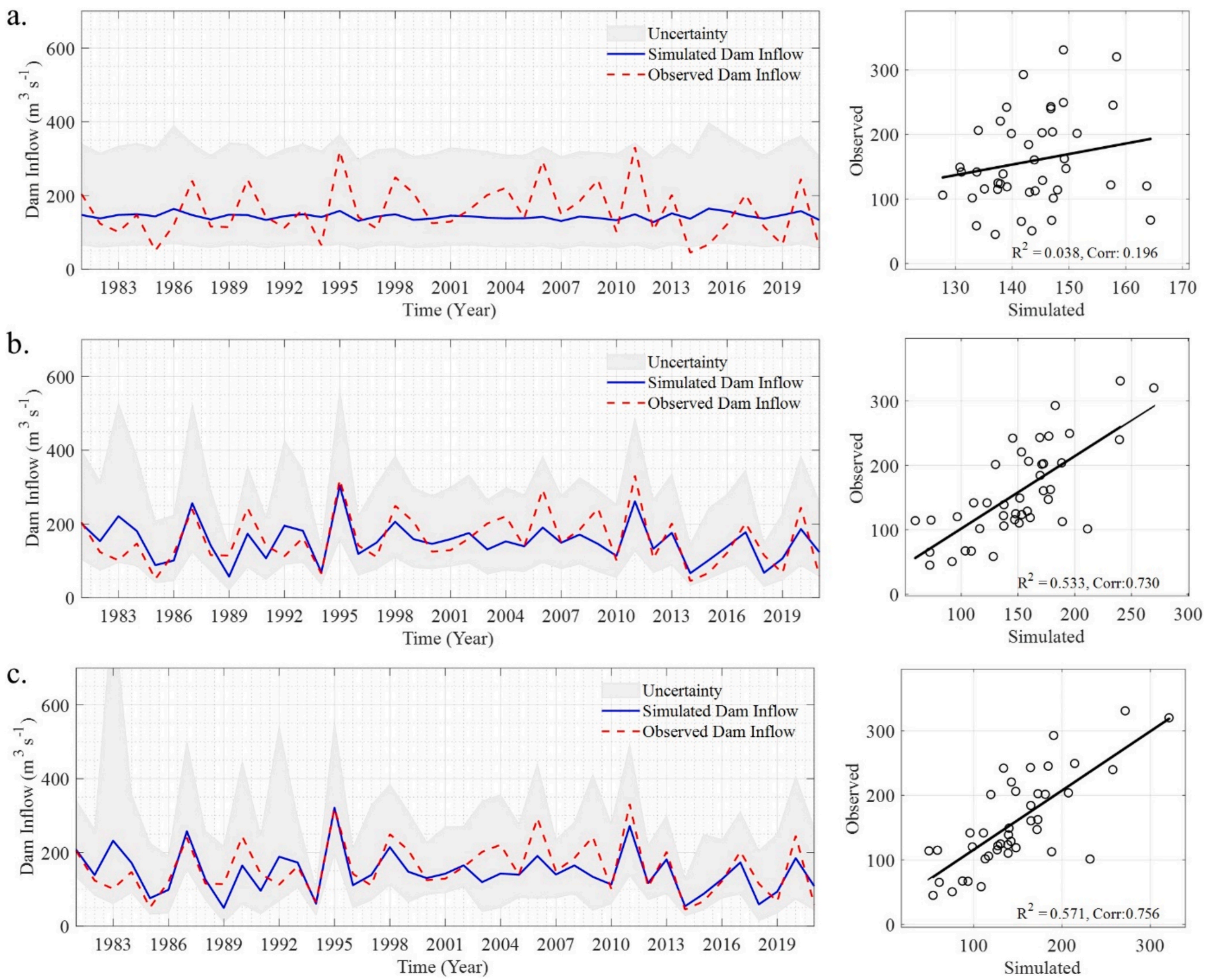

Fig. 9. Results of autoregressive models: (a) AR, (b) ARX, and (c) ARXSV models, showing time series and scatter plots with the observed streamflow data. Simulated dam inflow (blue solid line) from median posteriors with 95% credible intervals as uncertainty bounds (shaded grey), compared with observed dam inflow (red dashed line). (For interpretation of the references to colour in this figure legend, the reader is referred to the web version of this article.)

Table 3
Median and standard deviation values of posterior distributions associated with the autoregressive parameters.

Model	Posterior Medians (standard deviation)							
	α_1	α_2	β_1	β_2	γ_1	δ_1	δ_2	τ
AR	5.622	–0.132	–	–	–	–	–	–
	(0.787)	(0.158)	–	–	–	–	–	–
ARSV	6.519	–0.299	–	–	–	1.712	0.283	0.762
	(0.713)	(0.138)	–	–	–	(0.399)	(0.202)	(0.247)
ARX$_1$	6.519	–0.295	0.111	–0.034	–	–	–	–
	(0.631)	(0.126)	(0.029)	(0.010)	–	–	–	–
ARX$_2$	5.700	–0.148	–0.225	–	–	–	–	–
	(0.703)	(0.141)	(0.067)	–	–	–	–	–
ARX	6.398	–0.256	0.071	–0.034	–0.119	–	–	–
	(0.641)	(0.128)	(0.038)	(0.010)	(0.076)	–	–	–
ARXSV	6.942	–0.374	0.0942	–0.037	–0.167	0.656	0.263	5.065
	(0.534)	(0.108)	(0.042)	(0.010)	(0.081)	(0.165)	(0.199)	(1.897)

stochastic volatility adds substantial value to the model. By effectively quantifying uncertainty and incorporating prior knowledge, the model yields more robust and reliable estimates, providing a higher level of confidence in the results.

5.2. Model validation

To further ensure the robustness and reliability of the autoregressive exogenous stochastic volatility (ARXSV) model, we employed the LOOCV method. This method involves creating as many models as there

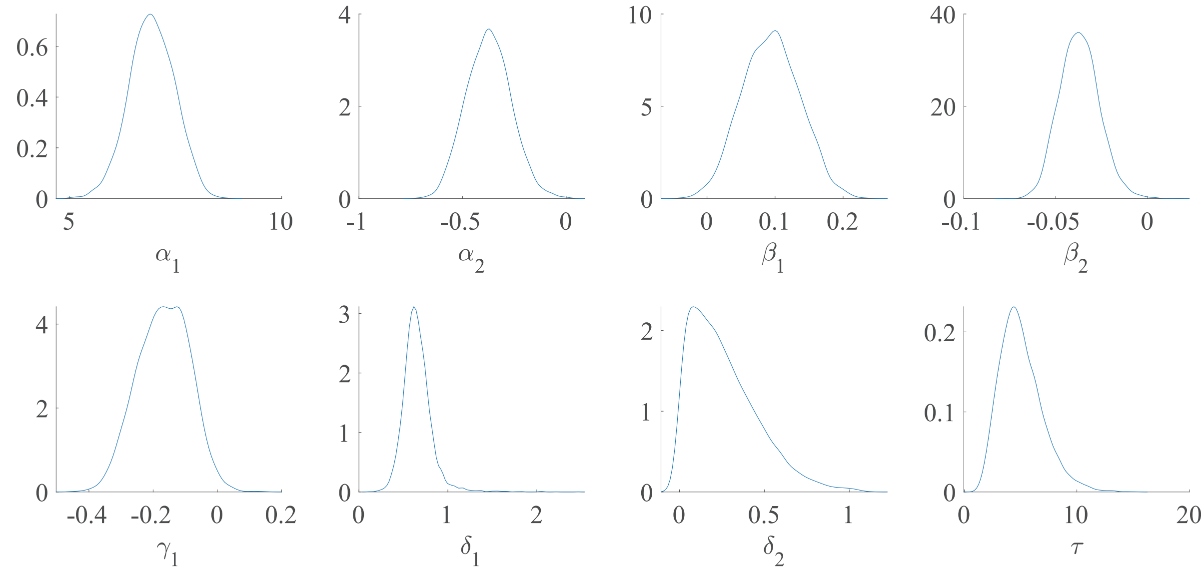

Fig. 10. Kernel density estimates of the marginal posterior distribution of the ARXSV parameter.

are data points, excluding one data point each time to serve as the validation set to understand the overall model performance. This method provides insights into how well the model generalizes to unseen data. In (Fig. 11), the LOOCV process is illustrated, where each model cycle results in a correlation value of the validation dataset. After completing the LOOCV procedure, we computed a correlation coefficient for each LOOCV iteration by comparing the predicted and observed values over the full study period and then averaged these correlation coefficients across all iterations. This yielded a mean correlation of 0.753, indicating reasonably good agreement between the model predictions and observations. The ARXSV model achieved consistently lower $\widehat{D}$ (3.0) and DIC (37.28) across the validation folds, indicating robust and superior probabilistic performance and ability to capture conditional, time-varying heteroscedasticity (Fig. 12).

6. Implications of summer seasonal flow forecasting for dam operation

The motivation for this study was prompted by recurring drought events in South Korea, often triggered by consecutive precipitation deficits. In the context of dam inflow prediction, statistical and dynamical modeling are two distinct approaches. Statistical modeling for dam inflow prediction primarily relies on historical data with relevant predictors, including the lagged values of streamflow and climate predictors. Thus, it involves scrutinizing past records to discern relationships between relevant variables (Wei and Watkins, 2011). These relationships are then used to create a statistical model, like the AR and ARX models described in this research. This type of model presents a transparent framework and is particularly useful when historical data are abundant. However, statistical models may not capture complex underlying physical processes, limiting their accuracy during extreme events (e.g., drought and flood). On the other hand, dynamic modeling employs physics-based models that simulate dynamic processes. In Fig. S1, a qualitative comparison is presented to contrast the outcomes of the ARXSV model with those of the dynamical Glosea5-ABCD model described in the Methodology Section 2.3.

This study conducted a comprehensive analysis of Soyang Dam drought severity by considering multiple time scales calculated at 1-month, 3-month, 6-month, and 12-month Standardized Streamflow Indices (i.e., SSI-1, SSI-3, SSI-6, and SSI-12). These time scales provide operationally relevant drought information, ranging from short-term inflow deficits (SSI-1) to seasonal conditions (SSI-3) and longer-term hydrological storage stress (SSI-6 and SSI-12). Drought severity is interpreted through the depth and duration of negative SSI values,

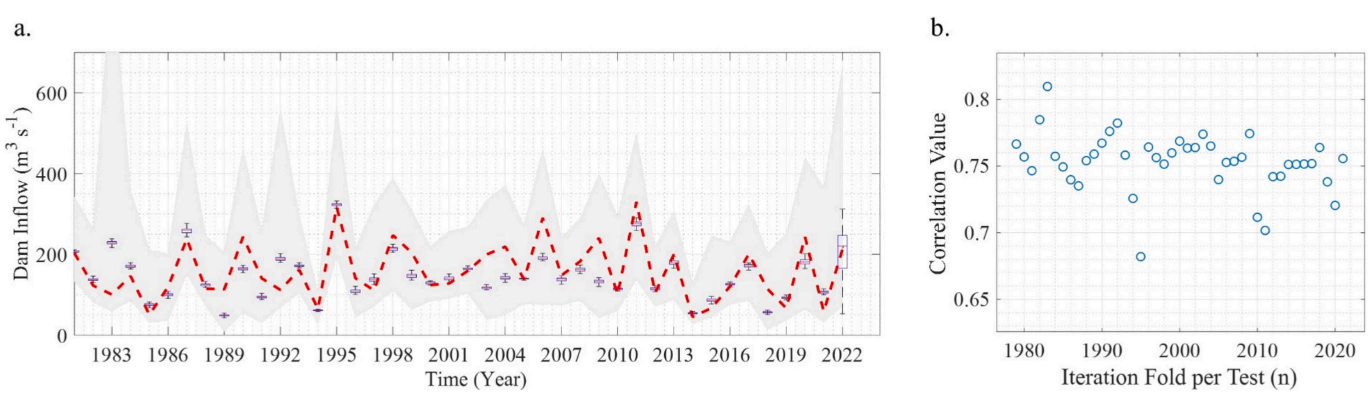

Fig. 11. Leave-one-out cross-validation (LOOCV) results for the ARXSV model showing (a) the observed dam inflow (red dashed line) and the concatenated out-of-sample posterior predictive summaries (box-plot). For each LOOCV iteration, the model is fitted to all years except one, and the held-out year is predicted; the blue solid line shows the median of the posterior predictive distribution for each held-out year, and the grey shading indicates the corresponding 95% credible interval. Panel (b) summarizes the resulting out-of-sample skill across held-out years to illustrate temporal stability; the 2022 point corresponds to the most recent out-of-sample fold. (For interpretation of the references to colour in this figure legend, the reader is referred to the web version of this article.)

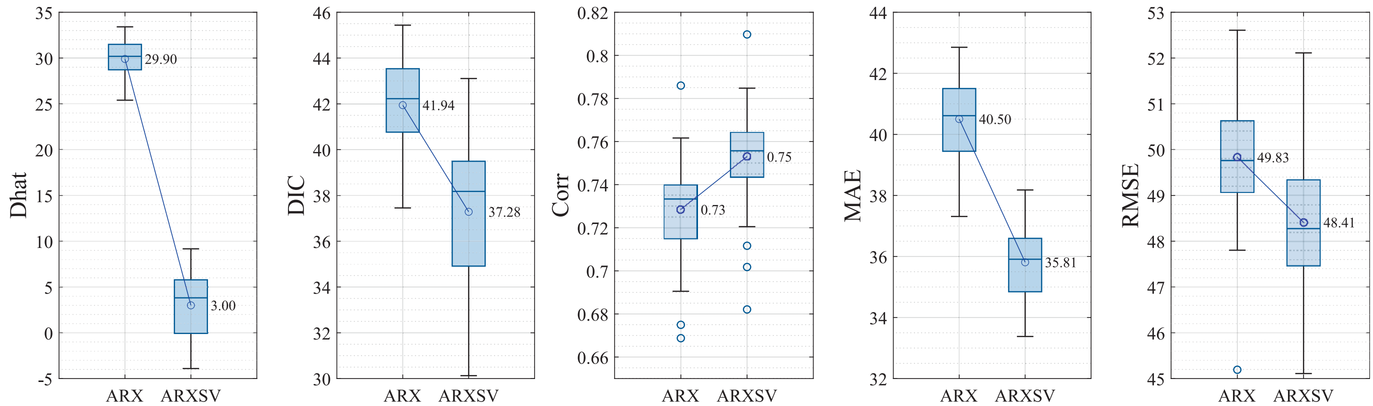

Fig. 12. Evaluation metrics ($\widehat{D}$, DIC, Corr, MAE, and RMSE) for the ARX and ARXSV models under LOOCV. Deviance-based criteria ($\widehat{D}$, DIC) quantify overall Bayesian model adequacy, while Corr, MAE, and RMSE summarize out-of-sample predictive performance based on LOOCV posterior predictive medians across held-out years.

which reflect increasingly rare low-flow conditions in the left tail of the streamflow distribution. For drought-relevant interpretation of seasonal JJA inflows, we focus on the 3-month accumulated index (SSI-3) in August derived from the ARXSV one-season-ahead forecasts (issued using pre-season spring climate predictors) and compare it with the corresponding JJA streamflow simulations from the GloSea5-ABCD model (Fig. S2). Here, Glosea5-ABCD is included to provide qualitative dynamical context for the target season rather than a lead-time-matched forecast for quantitative skill assessment. The black lines in the figure depict smoothed monthly SSI trends across 3-month accumulation periods. Notably, 1988, 1994, and 2014–2015 were identified as the three driest years (highlighted in gray) based on SSI-3 and SSI-6 accumulated periods, while 1990, 2003–2004, and 2020 stood out as pluvial or wet years (highlighted in blue).

Our findings align with previous research and reveal a common prolonged dry period between 1994 and 2014–2015 (Hong et al., 2016; Jung et al., 2011; Kwon et al., 2016). For the year 1988, the summer SSI-3 had a limited impact on the overall annual drought classification. This suggests that the drought conditions in 1988 were not predominantly experienced during the summer season but rather during the spring and winter of the preceding year, as the summer SSI-3 shows normal conditions. The years 1994 and 2014–2015 experienced moderate and extreme droughts, respectively, consequently showing a sharp decline in summer streamflow (Fig. 2). These events are well represented by the drought indices calculated from both the ARXSV and Glosea5-ABCD models.

In contrast, the wettest year identified in this study was 1990; it was extremely wet on an annual scale. However, the summer SSI values in that significant year were mildly wet and were detected to be normal by the ARXSV model. This phenomenon is also reported by Kim et al. (2019), who noted that the highest summer flows in the Soyang Dam during 1990 were not due to typhoon-induced precipitation. The wet years identified in 2003–2004 and 2021 can be explained by the high dam inflow, which resulted in mildly wet neutral conditions, with the ARXSV and GloSea5 models indicating a normal SSI-3.

In dam operation, statistical and dynamical approaches provide complementary perspectives. Statistical models (e.g., ARXSV) are effective for short- to medium-range prediction by leveraging historical observations to capture persistence and climate-driven signals, whereas dynamical models can offer a physically based large-scale climatic context that is informative for longer-horizon planning (So et al., 2020). Integrating statistical and dynamical streamflow predictions can help meet the proactive needs of dam operation and support decision-making (Yuan et al., 2015). In this study, however, the dynamical forecasts are used as a complementary physical context rather than as the primary focus of evaluation, given the limited hindcast period and the absence of extreme drought conditions during 2016–2022.

Our JJA seasonal statistical framework provides one-season-ahead guidance for dam-operation planning relevant to reliable water supply and flood management during the summer season. While the statistical model allows assessment of drought-relevant inflow predictability for years including 1994 and 2014–2015, the dynamical Glosea5-ABCD simulations are limited to 2016–2022, during which no extreme drought occurred in the study area. Accordingly, we present the dynamical forecasts as an illustrative physical context rather than a comprehensive drought-focused evaluation. A more rigorous integration and assessment of dynamical forecasts for drought-oriented dam operation would require longer hindcast records spanning extreme dry conditions, which we identify as an important direction for future research. Moreover, while the present framework focuses on forecasting seasonal inflow and subsequently deriving SSI-based drought indicators, an alternative approach would be to model SSI directly. This could potentially yield higher statistical skill for drought classification, as the model would be optimized for the standardized index itself. However, we deliberately prioritize inflow prediction because reservoir operation fundamentally depends on flow magnitude and timing. Based on the inflow forecasts, we then derive SST to represent above- and below-normal hydrologic conditions relative to the historical baseline.

7. Conclusion

In this study, we explored the performance of three autoregressive models—conventional autoregressive (AR), autoregressive with exogenous variables (ARX), and autoregressive exogenous with stochastic volatility (ARXSV)—in the context of predicting JJA seasonal streamflow. Our primary objective was to elucidate how these models responded to the autoregressive patterns and the integration of predictors derived from climate state variables. In particular, the ARX and ARXSV models incorporated the effects of preceding-season climate indices, representing the inclusion of pre-season Atlantic Sea surface temperature (SST_MAM), sea level pressure (SLP_MAM), and their combined effects, respectively. The results from this study offer valuable insights into the benefits of integrating large-scale climate teleconnections into an integrated Bayesian autoregressive framework, ultimately enhancing the accuracy of conventional autoregressive streamflow forecasting. Key concepts from this approach include:

1. This study places a significant emphasis on investigating the impact of teleconnections in the North Atlantic region on the Soyang Dam inflow. Notably, JJA streamflow shows a more pronounced correlation with SST and SLP during the MAM spring season. This climatic pattern is attributed to the combined influence of warm conditions in

the western tropical Pacific and anomalies in the North Atlantic during the spring season. Climate teleconnections in the North Atlantic Region, like the tripole SST and SLP, are both physically and statistically linked to Soyang Dam summer inflows, enabling a pre-season assessment of the climate's role in summer streamflow variability.
2. The ARXSV model demonstrated superiority in capturing the JJA streamflow variability compared to the stationary AR model. More specifically, noteworthy improvements in predictive accuracy were observed as we introduced climate information and stochastic volatility into the modeling framework. The ARXSV model, combining Bayesian inference with stochastic volatility, performed better across various metrics. The validation process further fortified the credibility of the ARXSV model. Employing the LOOCV method demonstrated the model's robustness, with a high average correlation coefficient indicating its capacity to generalize effectively to unseen data. Additionally, the credible intervals and posterior distribution analysis further highlighted the statistical significance and low uncertainty of the ARXSV model parameters.
3. Beyond performance metrics, our study also investigated the implications of drought prediction on dam operation. This study illuminated the strengths of both approaches by comparing the ARXSV model with a dynamical Glosea5-ABCD model. The ARXSV model emerged as a valuable tool for short- to medium-term forecasting, complementing the broader climatic insights offered by dynamical models. The integration of these two distinct modeling frameworks, as explored in our study, signifies a comprehensive approach for informed dam inflow management. The season-ahead summer Soyang Dam inflow model enables early detection of potential water shortages during dry periods in the Soyang Dam watershed, specifically during drought events in 1994 and 2014–2015.

In a time of increasing climate variability and hydrological challenges, the ARXSV model's transparent framework and strong performance make it an asset for both academic research and real-world applications for seasonal streamflow forecasting and hydrometeorological risk assessment in the challenging context of South Korea's recurring drought events.

CRediT authorship contribution statement

Pamela Sofia Fabian: Writing – original draft, Validation, Software, Methodology, Formal analysis, Data curation, Conceptualization. **Hemie Cho:** Methodology, Data curation, Conceptualization. **Yoo-Geun Ham:** Writing – review & editing, Supervision. **Hyun-Han Kwon:** Writing – review & editing, Validation, Supervision, Methodology, Investigation, Funding acquisition, Conceptualization.

Declaration of competing interest

The authors declare that they have no known competing financial interests or personal relationships that could have appeared to influence the work reported in this paper.

Acknowledgements

This work was supported by the Korea Environmental Industry & Technology Institute (KEITI) through "development of integrated asset management technology for water resources infrastructures to be incorporated in digital twins" (RS-2024-00337673), funded by the Korea Ministry of Climate, Energy and Environment (MCEE).

Appendix A. Supplementary data

Supplementary data to this article can be found online at https://doi.org/10.1016/j.jhydrol.2026.136255.

Data availability

Data will be made available on request.

References

Amarasekera, K.N., Lee, R.F., Williams, E.R., Eltahir, E.A.B., 1997. ENSO and the natural variability in the flow of tropical rivers. J. Hydrol. 200 (1–4), 24–39. https://doi.org/10.1016/S0022-1694(96)03340-9.
Harvey, A., Ruiz, E., Shephard, N., 1994. Multivariate stochastic variance models. Rev. Econ. Stud. 61 (2), 247–264. https://doi.org/10.2307/2297980.
Baek, H.-J., Kim, M.-K., Kwon, W.-T., 2017. Observed short- and long-term changes in summer precipitation over South Korea and their links to large-scale circulation anomalies. Int. J. Climatol. 37 (2), 972–986. https://doi.org/10.1002/joc.4753.
Berg, A., Meyer, R., Yu, J., 2004. Deviance information criterion for comparing stochastic volatility models. J. Bus. Econ. Stat. 22 (1), 107–120. https://doi.org/10.1198/073500103288619430.
Bollerslev, T., 1986. Generalized autoregressive conditional heteroskedasticity. J. Econ. 31, 307–327. https://doi.org/10.1016/0304-4076(86)90063-1.
Chiew, F.H.S., McMahon, T.A., 2002. Global ENSO-streamflow teleconnection, streamflow forecasting and interannual variability. Hydrol. Sci. J. 47 (3), 505–522. https://doi.org/10.1080/02626660209492950.
Choi, Y.-W., Ahn, J.-B., 2019. Possible mechanisms for the coupling between late spring sea surface temperature anomalies over tropical Atlantic and East Asian summer monsoon. Clim. Dyn. 53 (11), 6995–7009. https://doi.org/10.1007/s00382-019-04970-3.
D. J. Spiegelhalter, N.G.B., Bradley P. Carlin, Angelika Van Der Linde, 2002. Bayesian measures of model complexity and fit. J. R. Stat. Soc. 64(4). DOI:10.1111/1467-9868.00353.
Dawson, C.W., Abrahart, R.J., See, L.M., 2007. HydroTest: a web-based toolbox of evaluation metrics for the standardised assessment of hydrological forecasts. Environ. Model. Software 22 (7), 1034–1052. https://doi.org/10.1016/j.envsoft.2006.06.008.
Deng, K., Yang, S., Lin, A., Li, C., Hu, C., 2019. Unprecedented East Asian warming in spring 2018 linked to the North Atlantic tripole SST mode. Atmos. Oceanic Sci. Lett. 12 (4), 246–253. https://doi.org/10.1080/16742834.2019.1605807.
Engle, R.F., 1982. Autoregressive conditional heteroscedasticity with estimates of the variance of United Kingdom inflation. Econometrica 50 (4), 987–1007. https://doi.org/10.2307/1912773.
Forootan, E., et al., 2019. Understanding the global hydrological droughts of 2003-2016 and their relationships with teleconnections. Sci. Total Environ. 650 (Pt 2), 2587–2604. https://doi.org/10.1016/j.scitotenv.2018.09.231.
Gong, G., Wang, L., Condon, L., Shearman, A., Lall, U., 2010. A simple framework for incorporating seasonal streamflow forecasts into existing water resource management practices. JAWRA J. Am. Water Resour. Assoc. 46 (3), 574–585. https://doi.org/10.1111/j.1752-1688.2010.00435.x.
Guo, L., et al., 2021. Links between global terrestrial water storage and large-scale modes of climatic variability. J. Hydrol. 598. https://doi.org/10.1016/j.jhydrol.2021.126419.
Ham, Y.-G., Chikamoto, Y., Kug, J.-S., Kimoto, M., Mochizuki, T., 2017a. Tropical Atlantic-Korea teleconnection pattern during boreal summer season. Clim. Dyn. 49 (7–8), 2649–2664. https://doi.org/10.1007/s00382-016-3474-z.
Ham, Y.-G., Hwang, Y., Lim, Y.-K., Kwon, M., 2017b. Inter-decadal variation of the Tropical Atlantic-Korea (TA-K) teleconnection pattern during boreal summer season. Clim. Dyn. 51 (7–8), 2609–2621. https://doi.org/10.1007/s00382-017-4031-0.
Han, H., Kim, D., Wang, W., Kim, H.S., 2023. Dam inflow prediction using large-scale climate variability and deep learning approach: a case study in South Korea. Water Supply 23 (2), 934–947. https://doi.org/10.2166/ws.2023.012.
Han, T., et al., 2019. The decadal variability of the global monsoon links to the North Atlantic climate since 1851. Geophys. Res. Lett. 46 (15), 9054–9063. https://doi.org/10.1029/2019gl081907.
Hobeichi, S., et al., 2024. How well do climate modes explain precipitation variability? npj Clim. Atmos. Sci. 7 (1). https://doi.org/10.1038/s41612-024-00853-5.
Hong, I., Lee, J.-H., Cho, H.-S., 2016. National drought management framework for drought preparedness in Korea (lessons from the 2014–2015 drought). Water Policy 18 (S2), 89–106. https://doi.org/10.2166/wp.2016.015.
Hong, J., et al., 2020. Development and evaluation of the combined machine learning models for the prediction of dam inflow. Water 12 (10). https://doi.org/10.3390/w12102927.
Hidalgo, H.G., Dracup, J.A., 2003. ENSO and PDO effects on hydroclimatic variations of the Upper Colorado River Basin. J. Hydrometeorol. 4, 5–23. https://doi.org/10.1175/1525-7541(2003)004%3C0005:EAPEOH%3E2.0.CO;2.
Ionita, M., Lohmann, G., Rimbu, N., 2008. Prediction of spring Elbe discharge based on stable teleconnections with winter global temperature and precipitation. J. Clim. 21 (23), 6215–6226. https://doi.org/10.1175/2008jcli2248.1.
Ionita, M., Nagavciuc, V., 2020. Forecasting low flow conditions months in advance through teleconnection patterns, with a special focus on summer 2018. Sci. Rep. 10 (1), 13258. https://doi.org/10.1038/s41598-020-70060-8.
Islam, F., Imteaz, M.A., 2020. Use of teleconnections to predict western australian seasonal rainfall using ARIMAX model. Hydrology 7 (3). https://doi.org/10.3390/hydrology7030052.
Jung, I.-W., Bae, D.-H., Kim, G., 2011. Recent trends of mean and extreme precipitation in Korea. Int. J. Climatol. 31 (3), 359–370. https://doi.org/10.1002/joc.2068.

Jung, J., Kim, H.S., 2022. Predicting temperature and precipitation during the flood season based on teleconnection. Geosci. Lett. 9 (1). https://doi.org/10.1186/s40562-022-00212-3.
Kang, H.-Y., Kim, J.-S., Kim, S.-Y., Moon, Y.-I., 2017. Changes in high- and low-flow regimes: a diagnostic analysis of tropical cyclones in the Western North Pacific. Water Resour. Manag. 31 (12), 3939–3951. https://doi.org/10.1007/s11269-017-1717-3.
Kim, C.-G., Lee, J., Lee, J.E., Kim, N.W., Kim, H., 2020a. Monthly precipitation forecasting in the Han River Basin, South Korea, using large-scale teleconnections and multiple regression models. Water 12 (6). https://doi.org/10.3390/w12061590.
Kim, H., Kim, T., Shin, J.-Y., Heo, J.-H., 2022. Improvement of extreme value modeling for extreme rainfall using large-scale climate modes and considering model uncertainty. Water 14 (3). https://doi.org/10.3390/w14030478.
Kim, J.-S., Jain, S., Kang, H.-Y., Moon, Y.-I., Lee, J.-H., 2019. Inflow into Korea's Soyang Dam: hydrologic variability and links to typhoon impacts. J. Hydro Environ. Res. 22, 50–56. https://doi.org/10.1016/j.jher.2019.01.001.
Kim, J.-S., Jain, S., Yoon, S.-K., 2012. Warm season streamflow variability in the Korean Han River Basin: links with atmospheric teleconnections. Int. J. Climatol. 32 (4), 635–640. https://doi.org/10.1002/joc.2290.
Kim, Y.T., So, B.J., Kwon, H.H., Lall, U., 2020b. A multiscale precipitation forecasting framework: linking teleconnections and climate dipoles to seasonal and 24-hr extreme rainfall prediction. Geophys. Res. Lett. 47 (3). https://doi.org/10.1029/2019gl085418.
Koralegedara, S.B., Huang, W.-R., Chiang, T.-Y., Bui-Manh, H., 2025. Springtime soil moisture variability and its changing environmental drivers: a CMIP6 multi-model ensemble analysis for the subtropical East Asian region. Geosci. Lett. 12 (1). https://doi.org/10.1186/s40562-025-00436-z.
Kwon, H.-H., Brown, C., Xu, K., Lall, U., 2009a. Seasonal and annual maximum streamflow forecasting using climate information: application to the three Gorges Dam in the Yangtze River basin, China. Hydrol. Sci. J. 54 (3), 582–595. https://doi.org/10.1623/hysj.54.3.582.
Kwon, H.-H., Khalil, A.F., Siegfried, T., 2008. Analysis of extreme summer rainfall using climate teleconnections and typhoon characteristics in South Korea. JAWRA J. Am. Water Resour. Assoc. 44 (2), 436–448. https://doi.org/10.1111/j.1752-1688.2008.00173.x.
Kwon, H.-H., Lall, U., Kim, S.-J., 2016. The unusual 2013-2015 drought in South Korea in the context of a multicentury precipitation record: inferences from a nonstationary, multivariate, Bayesian Copula Model. Geophys. Res. Lett. 43 (16), 8534–8544. https://doi.org/10.1002/2016gl070270.
Kwon, H.-H., Lall, U., Obeysekera, J., 2009b. Simulation of daily rainfall scenarios with interannual and multidecadal climate cycles for South Florida. Stoch. Env. Res. Risk A. 23 (7), 879–896. https://doi.org/10.1007/s00477-008-0270-2.
Kwon, M., Kwon, H.-H., Han, D., 2020. A hybrid approach combining conceptual hydrological models, support vector machines and remote sensing data for rainfall-runoff modeling. Remote Sens. (Basel) 12 (11). https://doi.org/10.3390/rs12111801.
Lee, D., Kim, H., Jung, I., Yoon, J., 2020. Monthly reservoir inflow forecasting for dry period using teleconnection indices: a statistical ensemble approach. Appl. Sci. 10 (10). https://doi.org/10.3390/app10103470.
Lee, J.-Y., et al., 2017. The long-term variability of Changma in the East Asian summer monsoon system: a review and revisit. Asia-Pac. J. Atmos. Sci. 53 (2), 257–272. https://doi.org/10.1007/s13143-017-0032-5.
Lee, J.H., Julien, P.Y., Thornton, C., Lee, C.H., 2019a. Large-scale climate teleconnections with South Korean streamflow variability. Hydrol. Sci. J. 65 (1), 57–70. https://doi.org/10.1080/02626667.2019.1617869.
Lee, M.-H., Im, E.-S., Bae, D.-H., 2019b. A comparative assessment of climate change impacts on drought over Korea based on multiple climate projections and multiple drought indices. Clim. Dyn. 53 (1–2), 389–404. https://doi.org/10.1007/s00382-018-4588-2.
Lee, S., Kim, J., 2021. Predicting inflow rate of the Soyang River Dam using deep learning techniques. Water 13 (17). https://doi.org/10.3390/w13172447.
Lettenmaier, A.F.H.A.D.P., 1999. Columbia River streamflow forecasting based on ENSO and PDO climate signals. J. Water Resour. Plann. Manage. 125 (6). https://doi.org/10.1061/(ASCE)0733-9496(1999)125:6(333).
Li, W., Maharjan, S., El-Askary, H., 2025. Atmospheric teleconnection patterns and hydrological whiplashes in the Western U.S. Sci. Rep. 15 (1), 21262. https://doi.org/10.1038/s41598-025-06087-6.
Lima, C.H.R., Lall, U., 2010. Climate informed monthly streamflow forecasts for the Brazilian hydropower network using a periodic ridge regression model. J. Hydrol. 380 (3–4), 438–449. https://doi.org/10.1016/j.jhydrol.2009.11.016.
Liu, Z., Alexander, M., 2007. Atmospheric bridge, oceanic tunnel, and global climatic teleconnections. Rev. Geophys. 45 (2). https://doi.org/10.1029/2005rg000172.
Ma, J., et al., 2025. Skillful seasonal predictions of continental East-Asian summer rainfall by integrating its spatio-temporal evolution. Nat. Commun. 16 (1), 273. https://doi.org/10.1038/s41467-024-55271-1.
McKee, T.B., Doesken, N.J., Kleist, J., 1993. The relationship of drought frequency and duration to time scales. Eighth Conference on Applied Climatology.
Meyer, R., Yu, J., 2000. BUGS for a Bayesian analysis of stochastic volatility models. Economet. J. 3 (2), 198–215.
Meyer, Y., 2000. BUGS for a Bayesian analysis of stochastic volatility models BUGS for a Bayesian analysis of stochastic volatility models. Econ. J. 3 (2), 198–215.
Modarres, R., Ouarda, T.B.M.J., 2013. Modelling heteroscedasticty of streamflow times series. Hydrol. Sci. J. 58 (1), 54–64. https://doi.org/10.1080/02626667.2012.743662.
Myoung, B., 2021. Recent trend of cold winters followed by hot summers in South Korea due to the combined effects of the warm western tropical Pacific and North Atlantic in spring. Environ. Res. Lett. 16 (8). https://doi.org/10.1088/1748-9326/ac1134.
Myoung, B., Rhee, J., Yoo, C., 2020. Long-lead predictions of warm season droughts in South Korea using North Atlantic SST. J. Clim. 33 (11), 4659–4677. https://doi.org/10.1175/jcli-d-19-0082.1.
Noh, G.-H., Ahn, K.-H., 2022. Long-lead predictions of early winter precipitation over South Korea using a SST anomaly pattern in the North Atlantic Ocean. Clim. Dyn. 58 (11–12), 3455–3469. https://doi.org/10.1007/s00382-021-06109-9.
Pektaş, A.O., Kerem Cigizoglu, H., 2013. ANN hybrid model versus ARIMA and ARIMAX models of runoff coefficient. J. Hydrol. 500, 21–36. https://doi.org/10.1016/j.jhydrol.2013.07.020.
Rimbu, N., Dima, M., Lohmann, G., Stefan, S., 2004. Impacts of the North Atlantic Oscillation and the El Niño–Southern Oscillation on Danube river flow variability. Geophys. Res. Lett. 31 (23). https://doi.org/10.1029/2004gl020559.
Rust, W., et al., 2021. Exploring the role of hydrological pathways in modulating multi-annual climate teleconnection periodicities from UK rainfall to streamflow. Hydrol. Earth Syst. Sci. 25 (4), 2223–2237. https://doi.org/10.5194/hess-25-2223-2021.
Seo, K.-H., Son, J.-H., Lee, S.-E., Tomita, T., Park, H.-S., 2012. Mechanisms of an extraordinary East Asian summer monsoon event in July 2011. Geophys. Res. Lett. 39 (5), n/a–n/a. https://doi.org/10.1029/2011gl050378.
Shabri, A., Suhartono, 2012. Streamflow forecasting using least-squares support vector machines. Hydrol. Sci. J. 57 (7), 1275–1293. https://doi.org/10.1080/02626667.2012.714468.
Singh, S., Abebe, A., Srivastava, P., Chaubey, I., 2021. Effect of ENSO modulation by decadal and multi-decadal climatic oscillations on contiguous United States streamflows. J. Hydrol.: Reg. Stud. 36. https://doi.org/10.1016/j.ejrh.2021.100876.
Slater, L.J., et al., 2023. Hybrid forecasting: blending climate predictions with AI models. Hydrol. Earth Syst. Sci. 27 (9), 1865–1889. https://doi.org/10.5194/hess-27-1865-2023.
Smith, T.J., Marshall, L.A., 2008. Bayesian methods in hydrologic modeling: a study of recent advancements in Markov chain Monte Carlo techniques. Water Resour. Res. 44 (12). https://doi.org/10.1029/2007wr006705.
So, J.-M., Lee, J.-H., Bae, D.-H., 2020. Development of a hydrological drought forecasting model using weather forecasting data from GloSea5. Water 12 (10). https://doi.org/10.3390/w12102785.
Sung, M.K., et al., 2006. A possible impact of the North Atlantic Oscillation on the East Asian summer monsoon precipitation. Geophys. Res. Lett. 33 (21). https://doi.org/10.1029/2006gl027253.
Tamaddun, K.A., Kalra, A., Ahmad, S., 2017. Wavelet analysis of western U.S. streamflow with ENSO and PDO. J. Water Clim. Change 8 (1), 26–39. https://doi.org/10.2166/wcc.2016.162.
Valipour, M., Banihabib, M.E., Behbahani, S.M.R., 2013. Comparison of the ARMA, ARIMA, and the autoregressive artificial neural network models in forecasting the monthly inflow of Dez dam reservoir. J. Hydrol. 476, 433–441. https://doi.org/10.1016/j.jhydrol.2012.11.017.
Wagena, M.B., et al., 2020. Comparison of short-term streamflow forecasting using stochastic time series, neural networks, process-based, and Bayesian models. Environ. Model. Software 126. https://doi.org/10.1016/j.envsoft.2020.104669.
Wang, H., Song, S., Zhang, G., Ayantobo, O.O., Guo, T., 2023. Stochastic volatility modeling of daily streamflow time series. Water Resour. Res. 59 (1). https://doi.org/10.1029/2021wr031662.
Wang, L., Ma, F., Liu, J., Yang, L., 2020. Forecasting stock price volatility: new evidence from the GARCH-MIDAS model. Int. J. Forecast. 36 (2), 684–694. https://doi.org/10.1016/j.ijforecast.2019.08.005.
Wei, W., Watkins, D.W., 2011. Probabilistic streamflow forecasts based on hydrologic persistence and large-scale climate signals in central Texas. J. Hydroinf. 13 (4), 760–774. https://doi.org/10.2166/hydro.2010.133.
Wu, Z., Li, J., Jiang, Z., He, J., Zhu, X., 2012. Possible effects of the North Atlantic Oscillation on the strengthening relationship between the East Asian Summer monsoon and ENSO. Int. J. Climatol. 32 (5), 794–800. https://doi.org/10.1002/joc.2309.
Wu, Z., Wang, B., Li, J., Jin, F.-F., 2009. An empirical seasonal prediction model of the East Asian summer monsoon using ENSO and NAO. J. Geophys. Res. 114 (D18). https://doi.org/10.1029/2009jd011733.
Yuan, X., Wood, E.F., Ma, Z., 2015. A review on climate-model-based seasonal hydrologic forecasting: physical understanding and system development. WIREs Water 2 (5), 523–536. https://doi.org/10.1002/wat2.1088.
Zeng, W., Song, S., Kang, Y., Gao, X., Ma, R., 2022. Response of runoff to meteorological factors based on time-varying parameter vector autoregressive model with stochastic volatility in arid and semi-arid area of Weihe River Basin. Sustainability 14 (12). https://doi.org/10.3390/su14126989.
Zha, X., Xiong, L., Guo, S., Kim, J.-S., Liu, D., 2020. AR-GARCH with exogenous variables as a postprocessing model for improving streamflow forecasts. J. Hydrol. Eng. 25 (8). https://doi.org/10.1061/(asce)he.1943-5584.0001955.
Zheng, F., Li, J., Li, Y., Zhao, S., Deng, D., 2016. Influence of the Summer NAO on the Spring-NAO-based predictability of the East Asian Summer Monsoon. J. Appl. Meteorol. Climatol. 55 (7), 1459–1476. https://doi.org/10.1175/jamc-d-15-0199.1.
Zhou, Z., Ren, J., He, X., Liu, S., 2021. A comparative study of extensive machine learning models for predicting long-term monthly rainfall with an ensemble of climatic and meteorological predictors. Hydrol. Process. 35 (11). https://doi.org/10.1002/hyp.14424.
Zuo, J., Li, W., Sun, C., Xu, L., Ren, H.-L., 2013. Impact of the North Atlantic sea surface temperature tripole on the East Asian summer monsoon. Adv. Atmos. Sci. 30 (4), 1173–1186. https://doi.org/10.1007/s00376-012-2125-5.